FOI
SWEDISH DEFENCE
RESEARCH AGENCY

FOI-R--0345--SE
December 2001
ISSN 1650-1942
Scientific report

Emil Hällstig, Mikael Lindgren and Lars Sjöqvist

Study of a nematic zero-twist liquid crystal spatial light modulator

Sensor Technology
SE-581 11 Linköping

SWEDISH DEFENCE RESEARCH AGENCY

Sensor Technology
P.O. Box 1165
SE-581 11 Linköping

FOI-R--0345--SE

December 2001

ISSN 1650-1942

Scientific report

Emil Hällstig, Mikael Lindgren and Lars Sjöqvist

Study of a nematic zero-twist liquid crystal spatial light modulator

Issuing organization	Report number, ISRN	Report type
FOI – Swedish Defence Research Agency Sensor Technology P.O. Box 1165 SE-581 11 Linköping	FOI-R--0345--SE	Scientific report
	Research area code 4. C4ISR	
	Month year December 2001	**Project no.** E3831, I0107
	Customers code 5. Commisioned Research	
	Sub area code 41 C4I	

Author/s (editor/s)	Project manager
Emil Hällstig Mikael Lindgren Lars Sjöqvist	Lars Sjöqvist
	Approved by Svante Ödman
	Scientifically and technically responsible Mikael Lindgren

Report title

Study of a nematic zero-twist liquid crystal spatial light modulator

Abstract (not more than 200 words)

This report describes a characterization of a commercial liquid crystal spatial light modulator (SLM). Several methods for determining optical properties of SLM's are discussed and evaluated. The methods have been tested both by simulations and by experimental studies.

The phase response of an SLM is the relation between the applied voltage and phase modulation. Due to the nature of liquid crystals this relation is non-linear. By using look-up table (LUT) the relation can be adjusted to give a more linear response. Look-up tables, which almost produce a linear phase response, have been constructed by studying the phase response of the SLM.

The effects of a non-linear response on laser beam steering and shaping were studied. For beam steering and shaping the optimized LUT improved the performance. The steering efficiency was increased with respect to the intensity in the first order diffraction peak. For beam shaping more of the power in the intended region and less outside was observed.

Keywords

Spatial light modulator, SLM, liquid crystal, beam steering, phase modulation

Further bibliographic information	Language English
ISSN 1650-1942	**Pages** 38 p.
	Price acc. to pricelist **Security classification**

Utgivare	Rapportnummer, ISRN	Klassificering
Totalförsvarets Forskningsinstitut - FOI	FOI-R--0345--SE	Vetenskaplig rapport
Sensorteknik	**Forskningsområde**	
Box 1165	4. Spaning och ledning	
581 11 Linköping	**Månad, år**	**Projektnummer**
	December 2001	E3831
	Verksamhetsgren	
	5. Uppdragforskning	
	Delområde	
	41 Samband med telekom	

Författare/redaktör	Projektledare
Emil Hällstig	Lars Sjöqvist
Mikael Lindgren	**Godkänd av**
Lars Sjöqvist	Svante Ödman
	Tekniskt och/eller vetenskapligt ansvarig
	Mikael Lindgren

Rapportens titel (i översättning)

Studie av nematisk vätskekristall SLM

Sammanfattning (högst 200 ord)

Den här rapporten beskriver en utvärdering av en kommersiell vätskekristall SLM (ljusmodulator). Flera olika metoder för att karakterisera och utvärdera optiska egenskaper hos SLM:er har studerats. Metoderna har testats med hjälp av simuleringar och experimentella resultat.

Fasresponsen hos en SLM beskriver relationen mellan pålagd spänning och fasmodulering av ljuset. Fasresponsen är vanligtvis icke-linjär vilket härrör från fysikaliska egenskaper hos vätskekristallmaterialet. Genom att använda en "look-up" tabell (LUT) kan ett nära linjärt samband för fasresponsen erhållas. En optimerad LUT som ger ett nästan linjär fasrespons har bestämts genom experiment.

Effekten av en icke-linjär fasrespons har också studerats med avseende på laserstrålstyrning och strålformning. Genom att använda en optimerad LUT ökades strålstyrningseffektiviteten. För strålformningstillämpningar erhölls mer ljus till den önskade "spatiella" region jämfört med bakgrunden.

Nyckelord

SLM, vätskekristall, strålstyrning, fasmodulering

Övriga bibliografiska uppgifter	Språk Engelska

ISSN 1650-1942	Antal sidor: 38 s.
Distribution enligt missiv	Pris: Enligt prislista
	Sekretess

Contents

1 INTRODUCTION

A spatial light modulator (SLM) enables an operator to alter the phase distribution of a wave front of a propagating light-wave. This can be made within a 3-dimensional volume, such as in a holographic element, using all-optical means to create a phase grating from interfering coherent optical beams. Such phase gratings can be used as optical data storage devices and various wavelength selective and/or diffractive spatial filters. Alternatively, an electro-optically active medium or similar can be used in which the phase response of a medium is controlled by electrical means. The latter principle, resulting in an electronic control of the phase front, can be very handy for applications where it comes to steer an altered wave front or by other means direct the propagated energy via an active (logical) feedback. Applications of electronically controlled SLM's are numerous, e.g., various display technologies, optical signal processing, adaptive optics, laser beam steering, switching and routing within free-space interconnects, etc. Several different types of phenomena have been utilized to obtain an electronically controlled SLM [1].

The early types utilized the electronic magneto-optic and electro-optic effects of bulk materials, giving a fast response times, however, the driving electric and magnetic usually needed to be quite large to achieve enough phase-response. Other techniques that also can be used are acousto-optic modulators. The latter being based on the intricate mechanical and electrical properties of piezo and ferro-electric media giving relatively fast responses (10's of MHz) at moderate driving voltages but the very nature of the 'acoustic wave' phenomenon limits their use to 'one-dimensional' control. Piezo-electric drivers used in conjunction with mirrors have been used to form phase modulators for adaptive optics. A serious drawback with the latter technology is the bulky driving electronics and high cost.

The development of modern spatial light modulator technology is directed towards pixelated structures in which the size of the pixel (or pixel-spacing) is becoming of the same scale as the wavelength of the light wave to be controlled. This means that also the diffraction properties of the device must be invoked in the design and analysis of components. Micromirrors and related MEMS (Micro Electro Mechanical Systems) technology has been known for some years and can be used for relatively fast (kHz) modulation with low losses. The first versions of these devices are optimized for display (projection) applications and therefore these are not well suited for phase control. Recently, micromirror devices for phase modulation have started to appear on the market.

The development in methods for fabrication of sophisticated semiconductor devices has led to several new methods to construct spatial light modulators. One promising technique is multiple quantum well modulators (MQW) that rely on the quantum-mechanical effects of thin-stacked semiconductor layers. The quantum confinement introduces new sharp absorption peaks. Applying an electric field can alter the spectral locations of these peaks by a mechanism usually referred to as quantum confined Stark effect (QCSE). By choosing light at an appropriate wavelength the MQW and the electric field can be used to modulate the light. The contrast ratio is though rather low (e.g. 3:1) but the speed can be up to tens of GHz.

Liquid crystals have extensively been used in display technology over the past 10 – 15 years and offers a feasible way of obtaining intensity contrast and/or phase control of light in the visible and in the NIR. The electrical modulation bandwidth (frame-rate) is, however, strongly related to the number of phase levels that are achievable. One generally divides these into analogue and binary. Binary FLC's are fast and can operate up to 10's of kHz. Using time multiplexing this is enough for giving good contrast in display applications, however, their binary nature make them useless in certain applications such as beam pointing and tracking. Analogue devices are usually based on nematic liquid crystals and due to their continuous response to external fields they can resolve many phase levels, typically 8–10 bits, on the expense of being comparably slow (switch time ca 1 ms). The traditional (zero-twist) nematic LC device is suitable for both phase and intensity modulation. Most of previous studies in literature describe the investigation of Twisted Nematic LCD SLM's that is a variant optimized for display applications. The reason is that these are cheap and easy to purchase due to their frequent use in commercial display devices. However properties of the two types are closely related so similar methods for characterization can be applied with only minor modifications (see for example the part about measuring the physical properties of the SLM).

The aim of this report was to investigate and find methods to characterize the optical modulation response of an SLM. As a demonstrative example the Zero-Twist Nematic LC was studied in several configurations. A complex relation between the voltage and the optical modulation could define the phase response of the SLM where both the amplitude and the phase could be altered. A linear response is important in several applications such as beam steering and optical signal processors. Some efforts were made to compensate for non-linearity in the phase response by optimizing a better look-up table than offered by the manufacturer.

2 OPTICAL PROPERTIES OF THE SLM

The optical phenomenon commonly used to achieve phase modulation of an optical wave propagating through a liquid crystal is the optically anisotropy or birefringence. This means that the liquid crystal acts like a retarder in order to control and modify the polarization state of a propagating light wave. It also means that other polarizing components are generally required in order to select different means of operation as well as in the optimization of the performance. We here start by giving a brief introduction to the function of a nematic liquid crystal as an active optical device.

2.1 Optical properties of the nematic liquid crystal

The nematic liquid crystal is a uniaxially birefringent material. The unique axis, in a uniaxial crystal this is both a crystal axis and an optical axis, is parallel to the *director* of the liquid crystal. This is usually along the average orientation of the long axis of the liquid crystal molecules. The useful property of the nematic liquid crystal is that, when an alternating electric field is applied over the liquid crystal, the optic axis will orient so as to align itself with the field. The strength of the electric field controls the ability to align the optic axis with the field. Removing the field, the material relaxes back to its original

equilibrium orientation. When used as a retarder the optic axis of the liquid crystal is aligned along a specific direction in the plane of the large walls containing the material. The orientation of a liquid crystal between two electrode layers and its relation to an incoming light beam polarized perpendicular or parallel to the optic axis is shown in Figure 1.

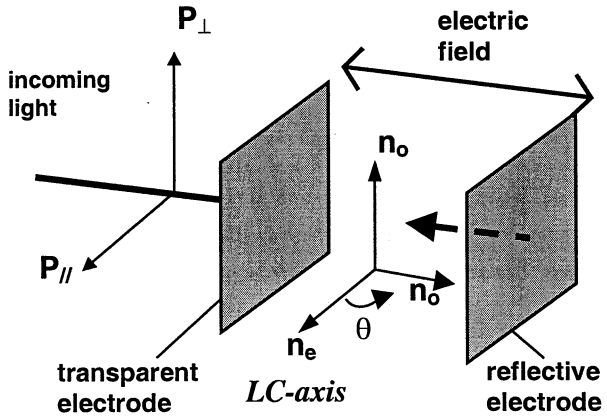

Figure 1 Schematic view of the liquid crystal orientation and the optic axis (director) for two possible impinging polarized light beams. By applying an electrical field the slow axis, n_e, is rotated the angle θ.

A more detailed scheme molecular alignment of a nematic liquid crystal and its relation to the applied electric field is shown in Figure 2. With no field applied the molecules are all oriented parallel with the alignment layer (top graphs). The polarization of light traversing through the cell, horizontal or vertical in left graph, will experience a delay when projected along the long axis of the molecules. This is referred to as the *slow axis* since the refractive index normally is larger for this polarization. Along the vertical axis the refractive index is smaller and consequently the light is traveling at higher velocity referred to as the *fast axis*. The two different refractive indices the light experiences with light polarized along the fast and slow axis usually are referred to as the ordinary and extraordinary, respectively, from the definitions used in crystal optics of uniaxial materials.

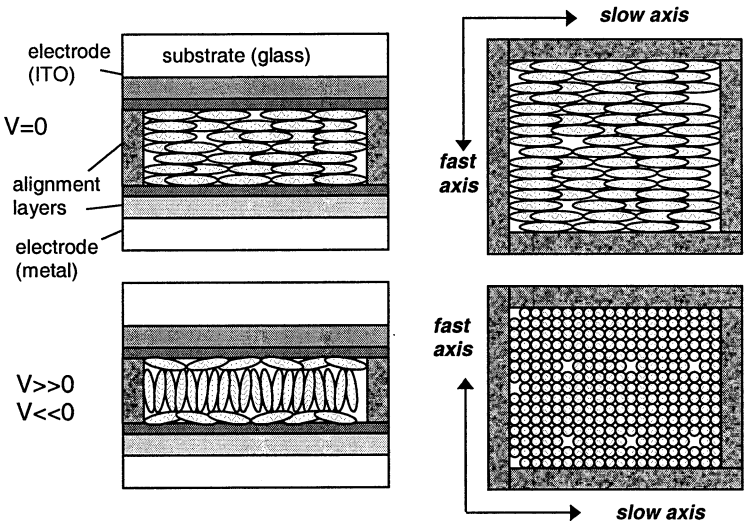

Figure 2 The molecular alignments used for operation of the nematic liquid crystal as a retarder, (top) without and (lower) with applied electric field. The left graph is for a side view through the cell. The right graph shows a view along the propagation of the optical beam.

With an applied voltage the molecules in the bulk of the LC cell tend to stand up changing the projection of the long axis of the molecules with respect to the horizontal polarization as shown in the lower graphs of Figure 2. Both axes, horizontal and vertical, will experience approximately the same phase-shift similar to that of the fast axis in the no-voltage case.

The response for a nematic liquid crystal can be theoretically calculated using expressions for the molecular rotation [2]. The molecular tilt θ due to an applied voltage V can be approximated by

$$\theta = \frac{\pi}{2} - 2\arctan\left[e^{-V}\right]. \qquad (1)$$

The molecular tilt then introduce a variation of the refractive index along the extraordinary axis which can be expressed as

$$\frac{1}{n_{eff}^{\,2}} = \frac{\cos^2\theta}{n_e^{\,2}} + \frac{\sin^2\theta}{n_o^{\,2}} \qquad (2)$$

where n_{eff} is the "effective" refractive index experienced for the slow polarization axis, n_o is the ordinary refractive index and n_e is the extraordinary refractive index when no voltage is applied. This curve is plotted for a voltage between 0 and 3 V, an ordinary refractive index of 1.5 and an extraordinary refractive index of 1.7 in Figure 3.

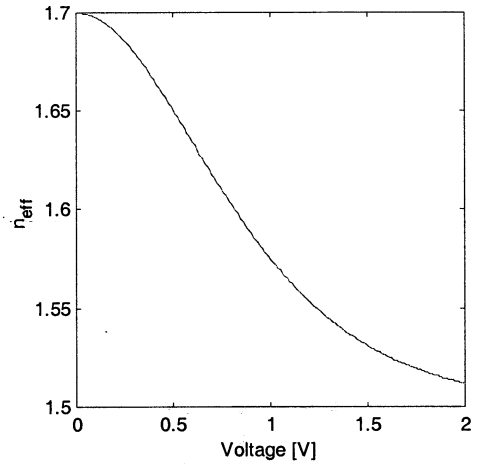

Figure 3 A calculated curve for the refractive index of a nematic LC versus applied voltage (eq. 1-2).

If the thickness of the cell and/or the birefringence (difference between n_e and n_o) is large enough it is possible to obtain a phase-shift of 2π between the polarizations of the slow and fast axes. Provided the response of the nematic liquid crystal material and the voltage is enough it is thus possible to continuously tune the phase-shift between 2π and 0. For an arbitrary polarization of the incoming light the voltage can be used to obtain any polarization state of the output provided the liquid crystal retarder is properly oriented.

In transmission mode the two electrodes used for changing the molecular orientation of the liquid crystal are made by transparent ITO (indium tin oxide). Consider that the phase difference between the fast and slow axes is set to give precisely a quarter of a wavelength when the liquid crystal is used in transmission mode. The retarder can hereby act as a converter between linearly and circularly polarized light as shown in Figure 4.

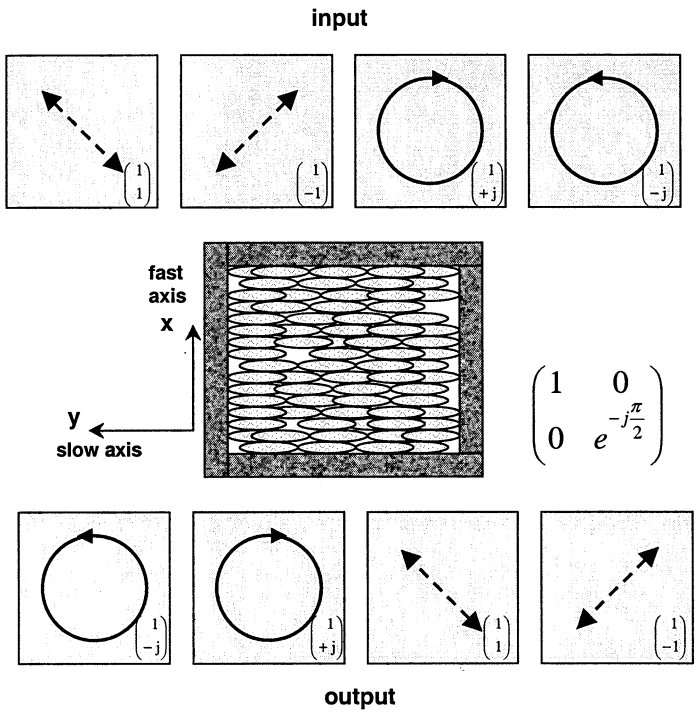

Figure 4 The conversion between linearly and circularly polarized light using a nematic liquid crystal as shown in Figure 2.1 as a quarter wave plate. The 2-by-1 and 2-by-2 matrices are the corresponding Jones vectors and the Jones matrix for the polarization states and the retarding component, respectively.

Note that when the input polarization is parallel to either the fast or slow axis no change of the polarization state is experienced. However, when aligned along the slow axis the applied voltage can be used to impose controlled phase retardation. Depending on the input polarization and auxiliary polarizing components, such as polarizers and wave plates, the liquid crystal can be used to obtain different types of amplitude and phase modulation.

Pure phase modulation can be accomplished with linearly polarized light aligned to the slow axis of the LC. Applying an electric field will then only alter the phase of the light. If the incoming light is linearly polarized at an angle α to the slow axis coupled amplitude and phase modulation can be achieved. Jones algebra can be used to predict the behavior of the modulation [3].

2.2 Jones algebra analyzes of a reflective LC cell

Define the coordinate system according to Figure 5 where the polarizer has been rotated an angle α from the y axis and the slow axis of the LC is parallel with the y axis throughout the cell.

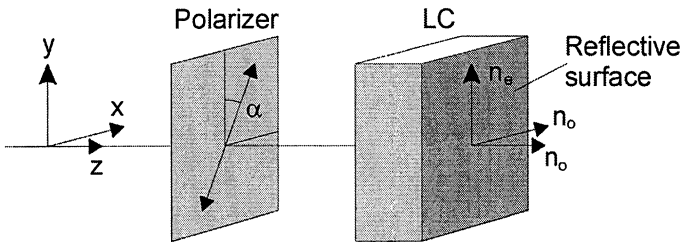

Figure 5 Schematic of the polarizer and LC cell.

Assume totally randomly polarized incoming light propagating in the z direction. After the polarizer the light can be expressed as the normalized Jones vector

$$\overline{E}_{in} = \begin{bmatrix} E_x \\ E_y \end{bmatrix} = \begin{bmatrix} \cos\alpha \\ \sin\alpha \end{bmatrix}. \tag{3}$$

When used in reflection mode one of the electrode layers is made by metal with high reflectance, such as aluminum or silver. If the LC is orientated as in the figure the light will pass through the liquid crystal twice. The Jones matrix can describe the first passage, before the reflection

$$\tilde{L}C(\beta) = \begin{bmatrix} 1 & 0 \\ 0 & e^{-j\beta} \end{bmatrix}., \tag{4}$$

where β is the phase delay due to the birefringence. The phase delay will depend on the refractive indices, the wavelength λ and the thickness d as

$$\beta = \frac{\pi d}{\lambda}\left(n_{eff}(V) - n_o\right). \tag{5}$$

After the reflection the light will pass through the LC again. If the liquid crystal is reciprocal the coupling from for example the x component to the y component for the forward pass through the device will be equal to the coupling from the y component to the x component on the reverse pass. The reverse pass can then be described in Jones algebra as the transpose of the Jones matrix for the forward pass [4].

The tangential components of the electric field must be zero at a perfectly conducting boundary as the mirror. Because of this the electric field components have to be the negatives of their values before the reflection. If dropping this introduced phase factor of 180° the field components E_x and E_y will be the same as before the reflection if observed in the original (x,y) coordinate system. However, the direction of propagation will though be reversed. If the right hand coordinate system with propagation in the z direction should be maintained the z and x have to be reversed, see Figure 6.

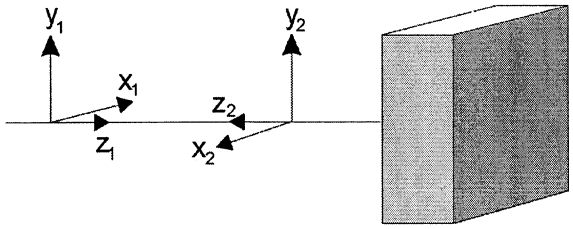

Figure 6 The two right-handed heads-on coordinate systems before and after the reflection.

The change in coordinate system can be expressed as the Jones matrix

$$\tilde{L}_{reflection} = \begin{bmatrix} -1 & 0 \\ 0 & 1 \end{bmatrix} \tag{6}$$

The Jones matrix for the complete LC with the reflection can be written as

$$\tilde{L}_{LC} = \tilde{L}_{reflection}\ \tilde{L}C^{T}\ \tilde{L}C \,. \tag{7}$$

When passing through the polarizer the second time the change in coordinate system inverts the sign of the angle to the optical axis. The passage of the polarizer can then be expressed as

$$\begin{aligned} L_{polarizer} &= \tilde{R}(\alpha)\,\tilde{P}\,\tilde{R}(-\alpha) \\ \tilde{R}(\alpha) &= \begin{bmatrix} \cos\alpha & \sin\alpha \\ -\sin\alpha & \cos\alpha \end{bmatrix} \\ \tilde{P} &= \begin{bmatrix} 0 & 0 \\ 0 & 1 \end{bmatrix}. \end{aligned} \tag{8}$$

The final transmittance of this set-up depending on the angle α and the phase delay of one passage β is then

$$\overline{E}_{out} = \tilde{R}(\alpha)\,\tilde{P}\,\tilde{R}(-\alpha)\,\tilde{L}_{reflection}\ \tilde{L}C(\beta)^{T}\ \tilde{L}C(\beta)\,\overline{E}_{in} \,. \tag{9}$$

In Figure 7 the calculated intensity is plotted versus the phase of the transmitted light.

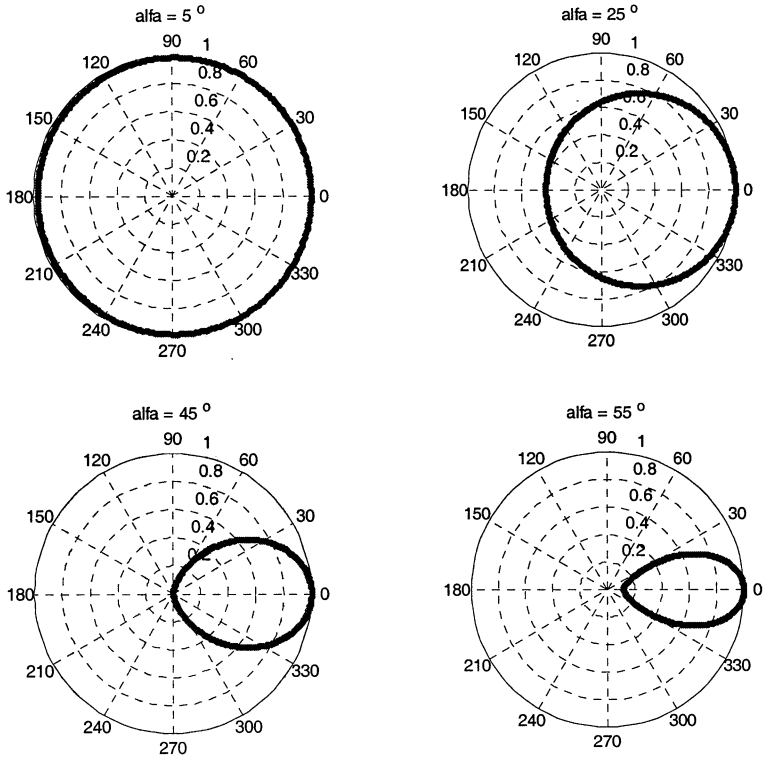

Figure 7 Polar plots of the coupled phase/amplitude modulation for four different angles α of the polarizer. Each modulation curve is plotted for a phase delay, β, of magnitudes between 0 and π.

As concluded earlier polarized light parallel to the y-axis give pure phase modulation. Amplitude modulation with full contrast is achieved when the polarizer is rotated 45° to the y-axis.

2.3 Method to measure the birefringence and rotation of the LC

A method to measure the orientation of the molecular director at the input side, the birefringence, the twist angle and an intensity scale factor of an arbitrary twisted-nematic LC, has been described previously [2]. The technique relies on the relative rotation of two polarizers, one placed in front of and the other after the SLM. The measurement is conducted by monitoring the transmitted intensity with the polarizers perpendicular and parallel to each other. Using Jones algebra together with non-linear curve fitting the unknown parameters can be determined. Ambiguities can arise using this procedure, however, by the additional use of several wavelengths it is possible to obtain a unique solution as reported by Davis et al. [5]. A simple technique for determining the extraordinary axis based on the fact that they had a nonuniform electric field over each pixel has been described [6].

The technique for characterization of the twisted nematic LC can also be adjusted for evaluation of the optical properties of a zero-twist nematic SLM as will be shown below.

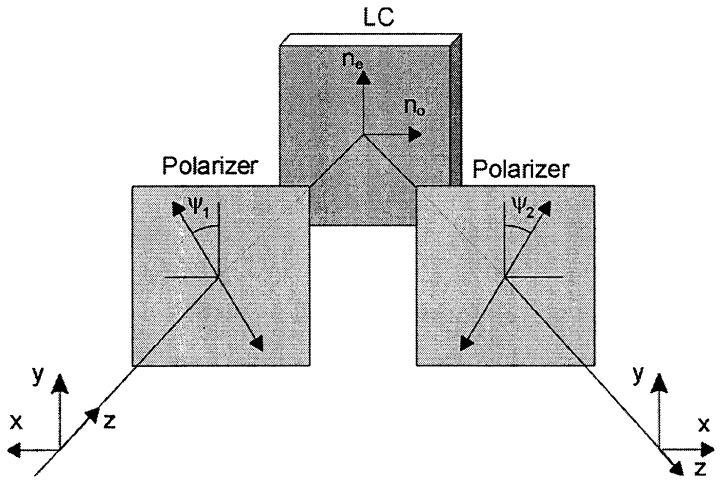

Figure 8 Schematic of set-up for characterization of the SLM.

Assume that the SLM is placed between two polarizers as in Figure 8. The y-axis is defined as the unknown extraordinary axis of the SLM and the transmission angles of the polarizers as ψ_1 and ψ_2. The normalized field incident to the SLM is represented by

$$\overline{E}_{before\ SLM} = \tilde{R}(\psi_1)\begin{bmatrix}0\\1\end{bmatrix}. \tag{10}$$

The electric field, E_{out}, after the last polarizer can then be written as

$$\overline{E}_{out} = \tilde{P}\,\tilde{R}(-\psi_2)\,\tilde{SLM}(\beta)\,\tilde{R}(\psi_1)\begin{bmatrix}0\\1\end{bmatrix} \tag{11}$$

where the Jones matrices for the polarizer (P), rotation (R) and the SLM are defined as

$$\begin{aligned}\tilde{P} &= \begin{bmatrix}0 & 0\\ 0 & 1\end{bmatrix}\\ \tilde{R}(\psi) &= \begin{bmatrix}\cos\psi & \sin\psi\\ -\sin\psi & \cos\psi\end{bmatrix}\\ \tilde{SLM}(\beta) &= \begin{bmatrix}1 & 0\\ 0 & e^{-j\beta}\end{bmatrix}.\end{aligned} \tag{12}$$

Observe that the final vector, E_{out}, is in the same coordinate system as the second polarizer. This is not a problem because only the intensity is measured. Equation (11) is used to calculate the resulting E field

$$\overline{E}_{out} = \begin{bmatrix} 0 \\ \sin(\psi_2)\sin(\psi_1) + \cos(\psi_2)\cos(\psi_1)e^{-j\beta} \end{bmatrix}. \quad (13)$$

The transmission is then given by

$$\begin{aligned} T &= real\{\overline{E}_{out}\}^2 + imag\{\overline{E}_{out}\}^2 = \\ &= \frac{1}{4}[\cos(\psi_2+\psi_1) - \cos(\psi_2-\psi_1) + \cos\beta(\cos(\psi_2+\psi_1) + \cos(\psi_2-\psi_1))]^2 + \\ &+ \frac{1}{4}\sin^2\beta[\cos(\psi_2+\psi_1) + \cos(\psi_2-\psi_1)]^2 \end{aligned} \quad (14)$$

where real{} and imag{} denotes the real and imaginary part of the field. If the orientation of the optical axes of the polarizers are perpendicular ($\psi_1 + \psi_2 = \pi/2$) or parallel ($\psi_1 = -\psi_2$) during the rotation the expression can be simplified to

$$\begin{aligned} T_{parallel} &= \frac{1}{4}[1 - \cos 2\psi + \cos\beta(1 + \cos 2\psi)]^2 + \frac{1}{4}\sin^2\beta[1 + \cos 2\psi]^2 \\ T_{perpend} &= \frac{1}{4}[\sin(-2\psi)(1 - \cos\beta)]^2 + \frac{1}{4}\sin^2\beta\sin^2(-2\psi) \end{aligned} \quad (15)$$

Important to note in these expressions is that the intensity varies as a function of twice the rotated angle and that the phase delay determines the amplitude of the variation. No phase delay will result in zero amplitude and no variation while a phase delay of π will give an amplitude of one. The ordinary and extraordinary axes can be found by study of the intensity while rotating the polarizers. It will not be possible to determine which axis that is the extraordinary and ordinary, but it becomes rather obvious when trying to use the SLM. Each time the intensity reaches a maximum and the polarizers are parallel they are aligned with an optical axis. In the same manner the intensity has minima for angles when the polarizers are crossed.

The experimental set-up in Figure 9 includes a reflection at an angle of incidence that is different from zero. This fact causes the reflection to be different for p and s polarised light according to the reflection equations of Fresnel. Hence the formulas presented here have to be adjusted with the reflection properties. In chapter 5 measured data are compared with these expressions.

3 EXPERIMENTAL PROCEDURES

3.1 General

The SLM investigated in this study was a Zero-Twist Nematic LC SLM purchased from BNS (Boulder Nonlinear System Inc) with 128x128 pixels that can be controlled digitally in a voltage range of 0 to 5 V with 7 bits resolution. The fill factor is 60% and the pixel

pitch is 40 μm, giving an active region of 5.12 x 5.12 mm. The SLM is of 'reflective' type meaning that the light make two passes through the active material. The phase response is obtained by aligning the liquid crystal to make light polarized along the vertical axis sensitive to the voltage over the pixels, each pixel being addressed individually. The phase delay can be varied in 128 levels between 0 and 2π at the design wavelength, λ=633 nm. Because the voltage applied on a LCD pixel is not linear to the resulting phase delay the BNS software can use different look-up tables (LUT). These tables give the relation between a pixel value and the applied voltage.

A HeNe laser operating at 632.8 nm wavelength and in addition wave plates, polarizers and other conventional optical components were used to investigate the performance and applications of the SLM. A 10-bits 944 x 860 pixels PULNIX CCD camera was used to record intensity patterns at specific positions in the optical set-up. In some cases the CCD camera was replaced by a silicon photodiode.

3.2 Phase and amplitude modulation

Two different experimental methods have been used (Figure 9). In the first experiments the angle between the incoming and outgoing wave was about ~20°. Subsequently, a non-polarizing beam splitter has been used to achieve an angle of incident that is perpendicular to the SLM plane. The introduction of the beam splitter give less transmittance but reduces the polarization change due to the oblique angle of incidence. Both methods can be used to generate pure phase modulation or coupled amplitude and phase modulation as discussed in a previous section. Since the orientation of the extraordinary axis of the SLM is known it can be mounted in such a way that the extraordinary axis is vertical and aligned with the optical axes of the polarizers. In this case pure phase modulation is obtained.

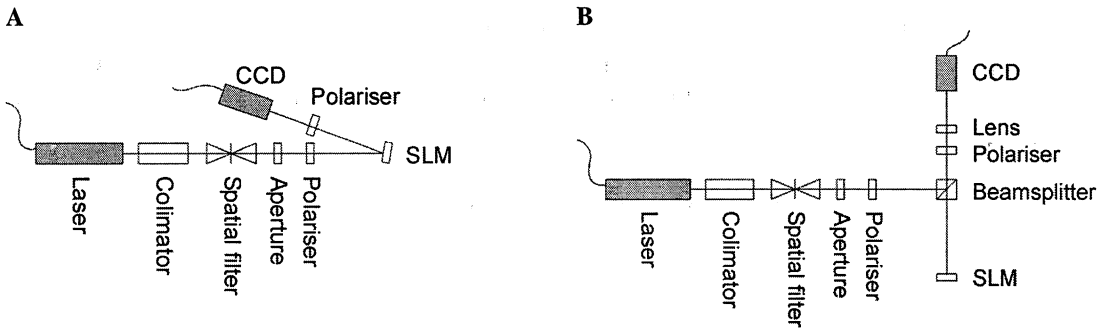

Figure 9 Experimental methods with tilted SLM in A and perpendicular incident light in B. Both set-ups give pure phase modulation when the polarizers are orientated in the same direction as the extraordinary axis of the SLM.

The camera and achromatic lens was placed so an image of the SLM was observed on the CCD. An image of symbols was downloaded to the SLM. Figure 10 illustrates an image of the SLM with the polarizers adjusted allowing pure phase or amplitude modulation.

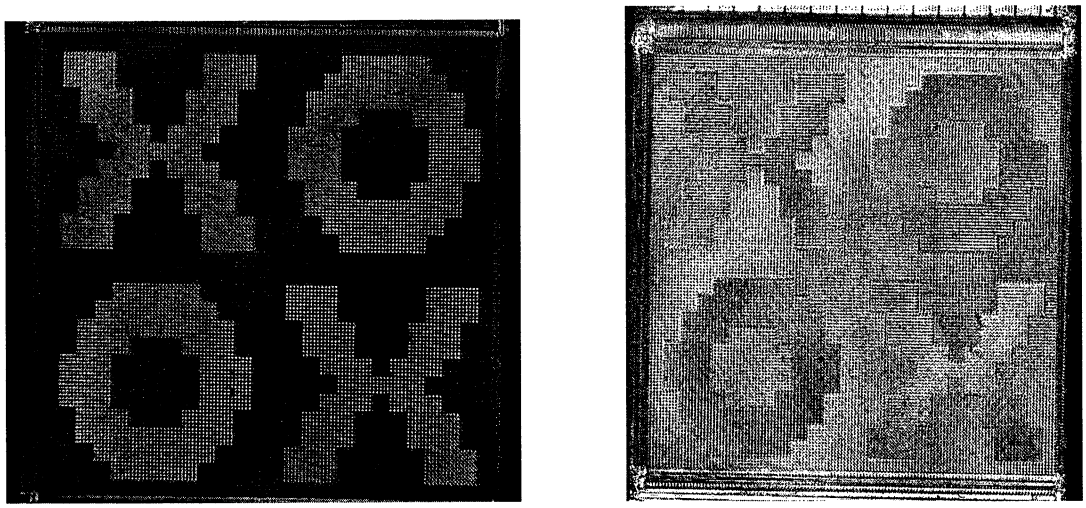

Figure 10 The SLM in the set-up for both amplitude (left) and phase modulation (right).

Ideally the image should be blank in the case of pure phase modulation. Interference in the system produces weak fringes diagonal over the SLM (Figure 10, left). Because of these intensity changes at some parts of the boundaries the image still can be recognized. However, the contrast is low which is expected for nearly pure phase modulation. In forthcoming sections it will be described how the phase response can be characterized and optimized by properly adjusting the signal for addressing the SLM pixels.

4 PHASE RESPONSE MEASUREMENT TECHNIQUES

The intensity response is straightforward to measure using for example a photodetector while varying the input signal. The phase response of a SLM is more cumbersome to measure, but several techniques that have been presented in the literature [2, 7, 8, 9, 10]. Some of the most utilized methods are briefly reviewed in this section. Emphasis has been on the techniques that are easy to set-up from an experimental point of view.

4.1 Interferometers

4.1.1 Mach-Zehnder interferometer

The most common method used to measure the phase response of an SLM is a Mach-Zender interferometer. For example, a Mach-Zender interferometer has been used to determine the phase modulation properties of a ferroelectric liquid crystal SLM [7]. A typical Mach-Zehnder interferometer is illustrated in Figure 11.

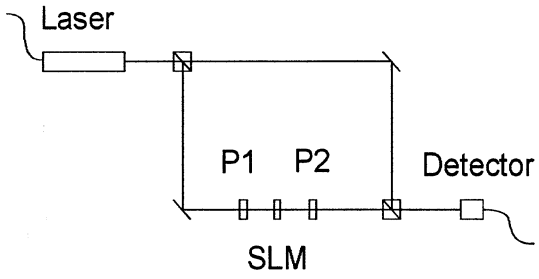

Figure 11 Mach-Zehnder interferometer for phase measurement of a SLM. P1 and P2 are two linear polarizers.

Transmissive SLM's are required using the Mach-Zender method. This architecture is also rather sensitive to the alignment and environmental conditions.

4.1.2 Michelson interferometer

If the design of the SLM is reflective a Michelson interferometer can be used [8]. A Michelson interferometer used for phase response measurements is depicted in Figure 12. Similar to the Mach-Zehnder interferometer this technique is also rather sensitive to the environmental conditions.

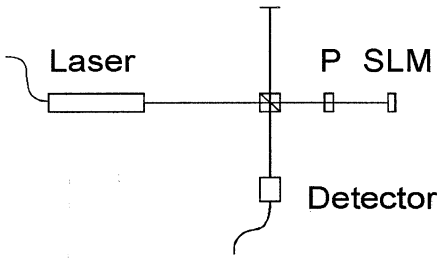

Figure 12 Michelson interferometer used for phase modulation measurement.

4.1.3 Common-path interferometer

One simple principle, called common-path interferometer, discussed by Bergeron and coworkers [9], is depicted in Figure 13. The mask with the two circular apertures is placed in front of the SLM. The far field diffraction pattern takes the form of a sinusoidal with a shift depending on the phase difference between the holes. By changing the value on the SLM behind one of the apertures and observing the diffraction pattern the phase modulation can be calculated. This set-up is simple and not so sensitive to the alignment procedure, since only the phase for a small area of the SLM is measured.

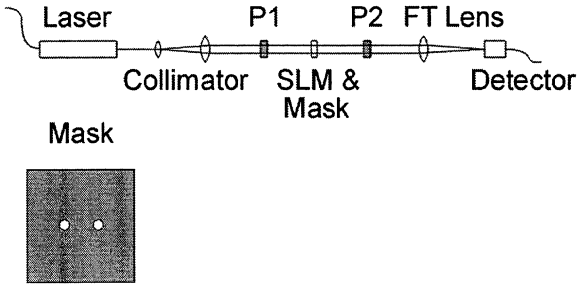

Figure 13 Common-path interferometer used for SLM phase measurement.

One other approach is to use a Ronchi ruling in a common-path interferometer as depicted in Figure 14. A high precision Ronchi component is required in this case.

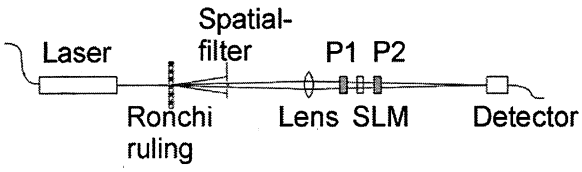

Figure 14 Common-path interferometer utilized with a Ronchi ruling [2].

4.2 Phase response measurement by interference in the SLM

Grother and Casasent have presented a method intended for easy evaluation of SLM's intended for optical correlators [10]. They use a simple imaging set-up similar to the one presented in Figure 9 and observe an interference pattern in the image of the SLM. A model of the SLM explaining the origin of the interference is shown in Figure 15.

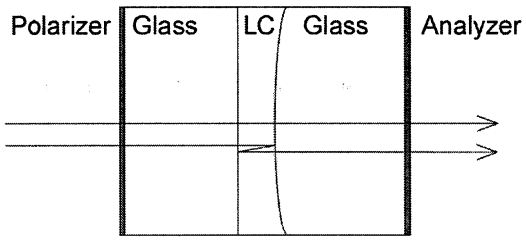

Figure 15 Simple model of an LC SLM.

By observing the interference pattern thickness variations over the SLM can be calculated. If different voltages are applied and the shift of the pattern is studied the phase response can be measured.

4.3 Phase response measurement using rotated polarizers

The phase response a zero-twist nematic LC SLM, with known orientation of the extraordinary axis, can be determined using two polarizers. Measurement of the transmitted intensity is performed for different pixel voltages when the two polarizers are parallel and

perpendicular to each other and ±45° with respect to the extraordinary axis. Observe that this method differs from the one described in chapter 2 ("Method to measure the birefringence and rotation of the LC"), because in this case the polarizers are fixed while in the former method they were rotated during the measurement. Using this method expression for the transmitted intensities can be calculated as [11]

$$T_{perp} = T_0 \sin^2 \frac{\delta}{2}$$
$$T_{par} = T_0 \cos^2 \frac{\delta}{2} \qquad (16)$$

where T_0 is the transmission and δ is the phase shift. If the sum of T_{perp} and T_{par} is taken as T_0, (16) can be used to calculate the phase from measured intensities. Simulations in MATLAB have been performed to validate this method in two different set-ups.

The phase response of the SLM exhibits a non-linear behavior as the function of the applied pixel voltage (Figure 16). The origin of this non-linearity is the response of the molecule due to the applied electric field, which affects the effective refractive index. Responses as those depicted in Figure 16 were used to calculate a look-up-tables (LUT) that could simulate the response of the SLM.

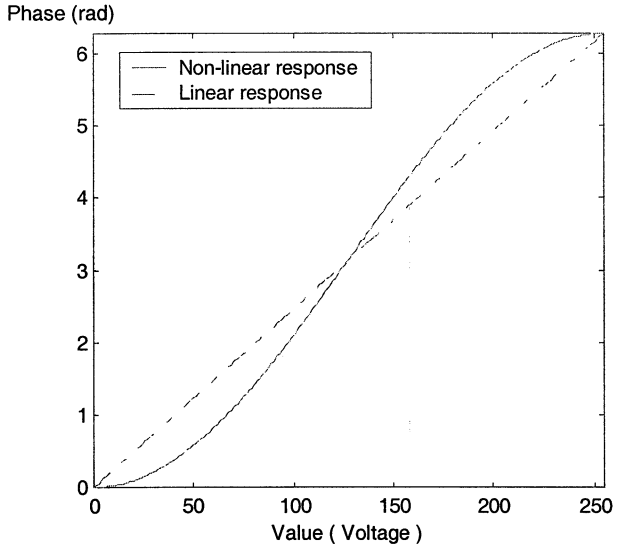

Figure 16 Linear and non-linear relation between phase modulation and the pixel voltage.

As mentioned above it has been shown that the total transmittance of the device could depend on the voltage due to interference effects [11]. To include this effect the amplitude of the field was multiplied with the transmission as a function of the applied pixel voltage. For a linear response between the applied pixel voltage and the phase delay the simulation of the calculated transmitted intensity is depicted in Figure 17.

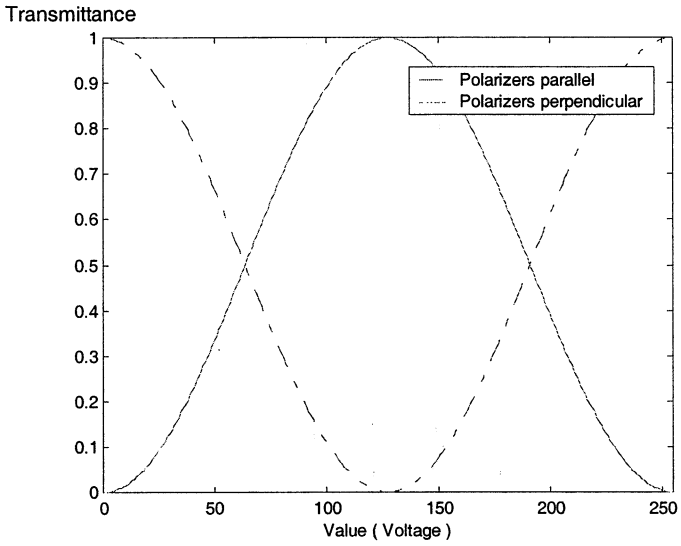

Figure 17 – Calculated transmitted intensity with parallel and perpendicular polarizers using a linear LUT.

To further investigate the method the angles of the polarizers were changed ±20°. This orientation depicts the situation when the orientation of the extraordinary axis is not known with high accuracy. Applying the errors in angles, a nonlinear LUT and amplitude disturbance a calculated transmitted intensity according to Figure 18 is obtained. It can be observed that the error sources change the intensity distribution, but the maximum and minimum are still on the same location. By normalizing the curves the effects from the errors in angles are cancelled. The amplitude disturbance is corrected by scaling each curve with to the inverse of the sum of the two curves. These corrections cause a decrease in accuracy of the response as observed in Figure 19, where the look-up-table has been plotted together with calculated values.

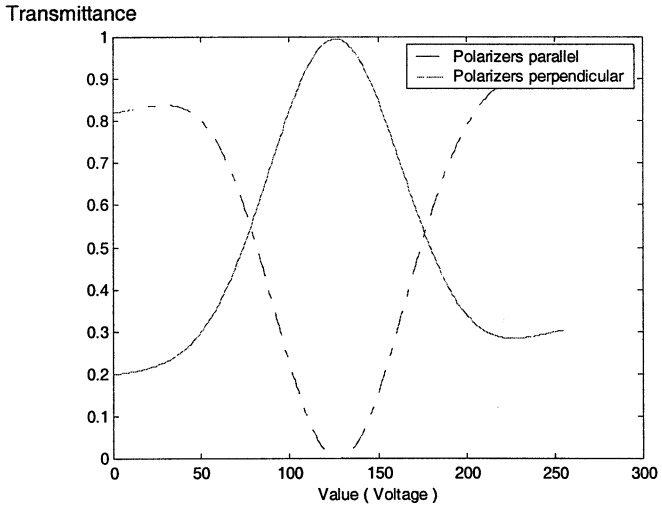

Figure 18 Simulated transmitted intensity for the set-ups with parallel and perpendicular polarizers.

Analyzing the results leads to the conclusion that maximum intensity always occurs when the phase modulation is π and the direction of the extraordinary axis of the device is located between the optical axes of the polarizers. In the same manner, the minimum occurs when the modulation is π and the polarizers are parallel. The reason for this behavior is that a SLM with a phase modulation of π acts like a half-wave retarder and rotates the linear polarized light around the extraordinary axis. Consequently, the SLM does not change the polarization state of the light.

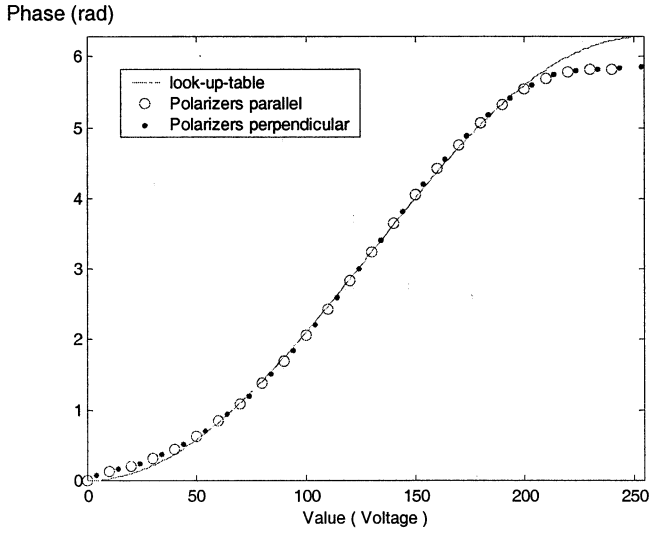

Figure 19 Simulated phase response.

The crossing of the two intensity curves (Figure 17) taking place at pixel values 64 and 192, indicate a phase modulation of $\pi/2$. This phase retardation produces circularly polarized light and the orientation of the second polarizer does not affect the transmitted intensity. In order to determine the phase accurately the polarizers should be directed at $\pm 45^{\circ}$. The method described in this paragraph is simple and the calculations show that the orientation of the extraordinary axis only has to be approximately known.

4.4 Phase response measurement by changing the amplitude of phase gratings

One method to determine the phase response without mechanical movement has been developed. It is based on studying far-field diffraction patterns while changing the amplitude of a phase grating. An expression for the diffracted efficiency for a stepped saw tooth formed phase grating has been derived by Dammann [12] and modified by Goodman [4]. The efficiency for different diffraction order can be written as

$$\eta_q = \sin c^2\left(\frac{q}{2^N}\right)\frac{\sin c^2\left(q-\frac{\phi_0}{2\pi}\right)}{\sin c^2\left(\frac{q-\frac{\phi_0}{2\pi}}{2^N}\right)} \tag{17}$$

where q is the order, ϕ_0 is the peak-to-peak phase difference and 2^N is the number of quantization levels. For a binary grating N is one and ϕ_0 represents the amplitude. By varying the height of the grating and measuring the intensities in the zero and first orders the following relation can be used to deduce the phase delay ϕ_0

$$\begin{aligned}\phi_0 &= 4\arccos\sqrt{\eta_0}\\ \phi_0 &= 4\arcsin\sqrt{\frac{\pi^2}{4}\eta_1}\end{aligned}. \tag{18}$$

It is recommended to measure the power in both the zero and in the first diffraction orders to increase the accuracy and make it possible to compensate for fluctuations in the total intensity.

4.5 Phase retrieval

The intensity distributions in two planes, often near- and far-field, phase retrieval algorithms can be used to reconstruct the original phase in the first plane. This phase distribution produces the observed intensity in the second plane. This technique has been used to determine the phase response of a ferroelectric SLM [13]. The intensity after the SLM was measured with incoherent illumination by scanning a pinhole after the device. In the far-field plane the intensities in the first 30 diffraction orders were measured using coherent light. One advantage of phase retrieval methods is that the spatial response is obtained. The disadvantage of phase retrieval algorithms is the existence of non-unique solutions. Another problem is that the intensity has to be measured in the two planes. Moreover, employing a scanning pinhole to monitor the intensity is tedious. A more attractive alternative is to use a high-resolution CCD to image the SLM and measure the far-field diffraction pattern. Some phase retrieval algorithms described in literature are briefly reviewed below [13,14,15].

4.5.1 Gerchberg-Saxton algorithm

The Gerchberg-Saxton algorithm reconstructs the phase from intensity measurements in each of the two domains [14]. The algorithm contains the following steps:

- Fourier transform (FT) an estimation of the object
- Replace the modulus of the result with the one measured in the Fourier domain

- Inverse FT the constructed estimation
- Replace the modulus of the result with the one measured in the object domain
- Iterate

4.5.2 Error-reduction algorithm

The error-reduction algorithm is a generalization of the Gerchberg-Saxton algorithm [13,15]. This method can be use if constraints in the domains are known. For example, in astronomy the intensity pattern in the Fourier domain is known and the object domain is known to be real. The algorithm contains the following steps:

- FT an estimation of the object
- Make the minimum changes to the result, which allows it to obey the Fourier domain constraints
- Inverse FT the constructed estimation
- Make the minimum changes to the result, which allows it to obey the object domain constraints
- Iterate

4.5.3 Adaptive Gerchberg-Saxton algorithm

To improve the convergence of the Gerchberg-Saxton algorithm several adaptive methods have been developed [13]. The idea of these methods is to take the previous estimate into account for each calculated new value. The modulation can be replaced by a weighted expression $W_n(x,y)$ which is calculated according to

$$W_n = W_{n-1}\left(\frac{\sqrt{I_{ref}}}{|G_n|}\right)^{0.2} \tag{19}$$

where I_{ref} is the reference intensity in the Fourier domain and G_n is the FT of the estimation in object domain.

5 EXPERIMENTAL RESULTS

5.1 Measurements of the birefringence and rotation of the SLM

The formulas derived in chapter 2 ("Method to measure the birefringence") were used to verify that the physical properties of a zero-twist SLM could be determined performing experimental measurements. The optical axes orientations of the polarizers were first determined. The angles of rotation were defined so when $\alpha = 0$ the polarizers were orientated vertically in the laboratory frame. The SLM was tilted around this vertical axis so at $\alpha = 0$ the light incident on the SLM was purely s-polarized. No voltage was applied to the SLM to keep it stable during the measurements. First the relation between the rotation

of the first polarizer and reflected intensity with the second polarizer removed was studied. This is necessary due to the unknown polarization of the light emitted by the laser and the reflection dependency of the polarization. As shown in Figure 20 the reflected intensity is dependent of the rotation of the first polarizer. This could be the effect if the light emitted from the laser is linearly polarized in the vertical direction or if almost no light at all is reflected at the SLM when the incident light is p-polarized.

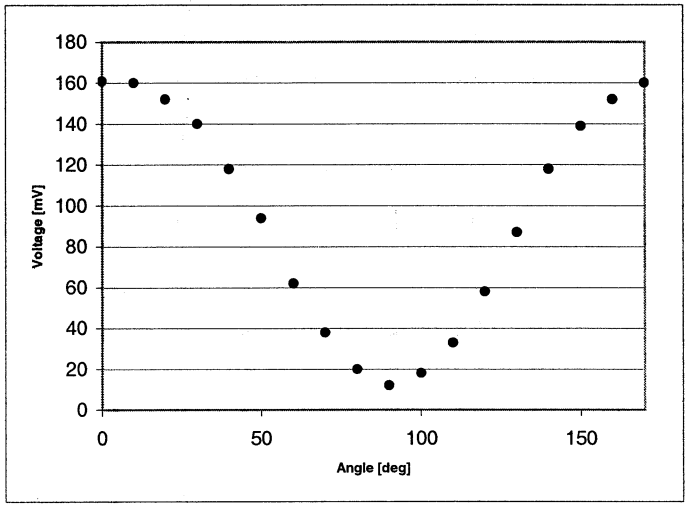

Figure 20 The voltage from the photodiode while the polarizer was rotated in front of the SLM.

As indicated by the experimental results shown in Figure 20 the intensity after the reflection at the SLM could be approximated by

$$I_{out} = \cos(\alpha) I_{in} \tag{20}$$

where I_{in} is the intensity after the polarizer.

The second polarizer was thereafter inserted in the set-up and both polarizers were aligned to be parallel. The voltage from the photodiode was measured while the polarizers were simultaneously rotated. The measurement was repeated for the polarizers perpendicular as shown in Figure 21. As expected from the discussion above the intensity shows variations proportional to $\cos(\alpha)$ from the polarization dependency of the reflection and to $\cos(2\alpha)$ due to the birefringence of the LC.

In chapter 2.3 expressions for the reflected intensity as a function of the orientation of two polarizers were derived. The theoretical expressions with the unknowns ψ and β can be fitted to the experimental data (Figure 21). Best agreement was obtained when $\psi = 8^{\circ}$ and $\beta = 2.24$.

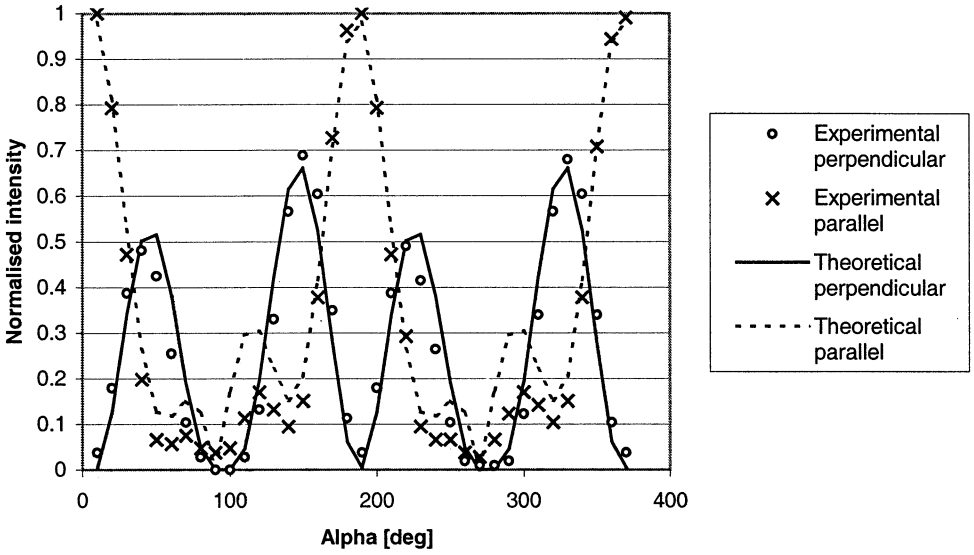

Figure 21 – Theoretical and experimental intensities with the values $\psi=8^{\circ}$ and $\beta=2.24$.

5.2 Measurements of the phase response

Some of the methods designed to analyze the phase response of SLM's were experimentally evaluated. The following methods were investigated:

- polarizers rotated $\pm 45^{\circ}$
- the phase grating method
- the use of interference

A non-linear response can be corrected by applying a look-up table. The two look-up tables provided by the manufacturer are plotted in Figure 22. Phase response measurements were conducted with both these LUT's.

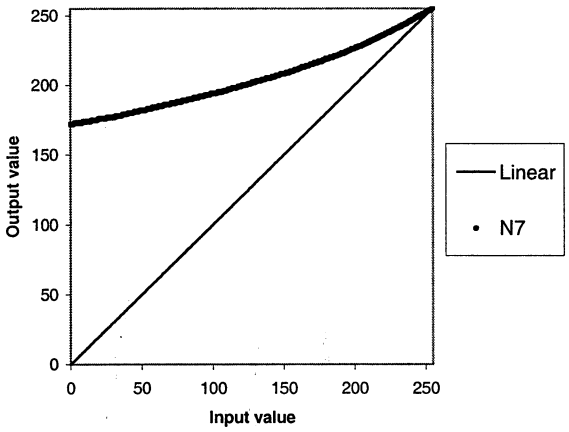

Figure 22 Look-up tables "Linear" and "N7".

5.2.1 Measurements of the phase response with rotated polarizers

As described earlier the polarizers are rotated 45° from the extraordinary axis of the liquid crystal to become either perpendicular or parallel. The reflected intensity is measured for a set of different pixel values on the SLM. For the ideal case the two set-ups will produce pure sinus and cosines responses. The variation of the reflected intensity was measured and the result using the linear LUT is shown in Figure 23.

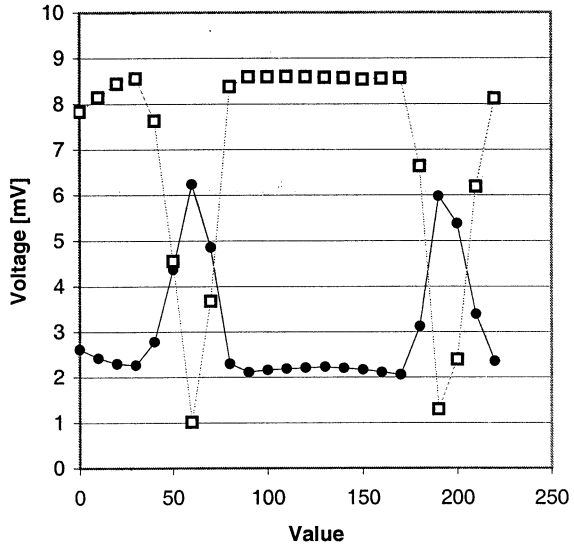

Figure 23 Signal versus the applied pixel value. Parallel (dots) and perpendicular (squares).

The phase can be calculated for each value using the theoretical expressions for the reflected intensity (Figure 24). In several points it is not possible to determine if the phase increase or decrease. The displayed curve has been constructed by assuming a increasing phase response and summing up the phase differences. The result is a maximum phase response of 4π, which is not true. This behavior is due to the fact that the 8^{th} bit only controls the dc-compensation. This means that values above 127 is only a mirror of the phase response below 127. The difference in phase delay between 0 and 127 is about 2π (one wavelength) as expected.

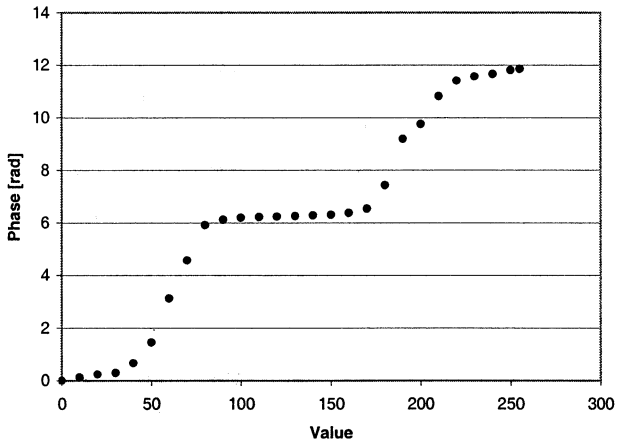

Figure 24 Calculated response for the linear LUT.

The intensity variations were also measured for the N7 LUT in order to compare the results with the linear LUT. In this case a cosine and sine relation between the reflected signal and the applied pixel value can be observed (Figure 25).

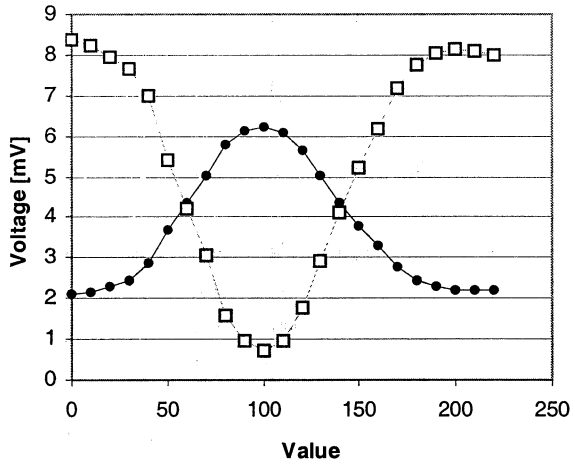

Figure 25 Signal versus the applied pixel value. Parallel (dots) and perpendicular (squares).

These results were used to calculate the phase response of the SLM (Figure 26). As observed in this case a better dynamic range is obtained. The relation between the applied pixel value and the phase response is still non-linear indicating that the N7 LUT is not optimal.

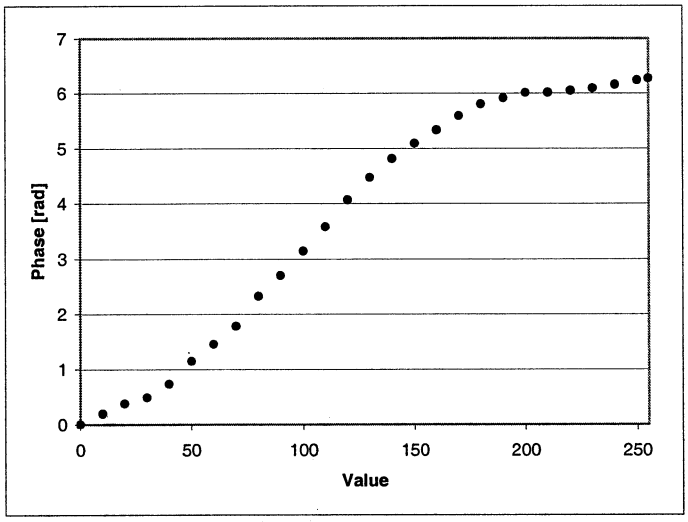

Figure 26 Calculated phase response for the N7 LUT.

5.2.2 Phase response by changing the height of a phase grating

By measuring the power in the zero and first diffraction orders the relation between the amplitude of a phase grating and the phase delay can be calculated. In Figure 27 the power in the diffraction orders are plotted versus the pixel value (amplitude of the phase grating). The intensity has been normalized so that the maximum power in the zero order corresponds to 100%. A grating with amplitude, which corresponds to a pixel value 115, results in a far-field pattern with maximum energy in the first order peaks.

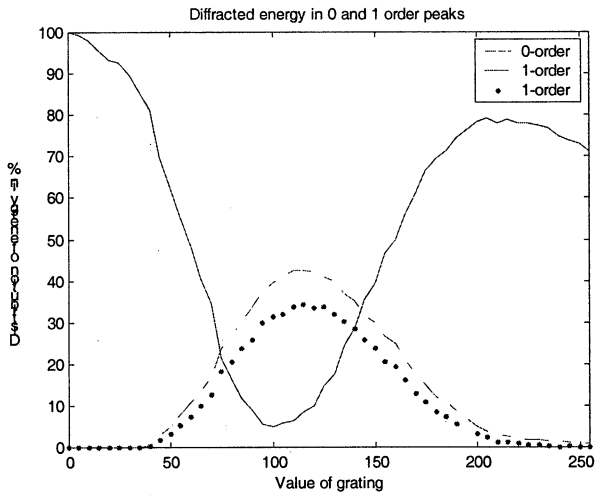

Figure 27 Diffracted power into the zero and the first orders versus the amplitude of the phase grating for the N7 LUT.

This corresponds to a grating of height π or a half wavelength, which theoretically predicts about 40% of the optical power into each of the ±1 diffraction, orders and no power in the zero order. The fact that the zero order does not vanish completely can probably be

attributed to the gaps between the pixels and presence of amplitude modulation. These results were used to calculate the phase response according to eq. (18). If the experimental results from the ±1 and zero orders are used the phase response can be calculated (Figure 28).

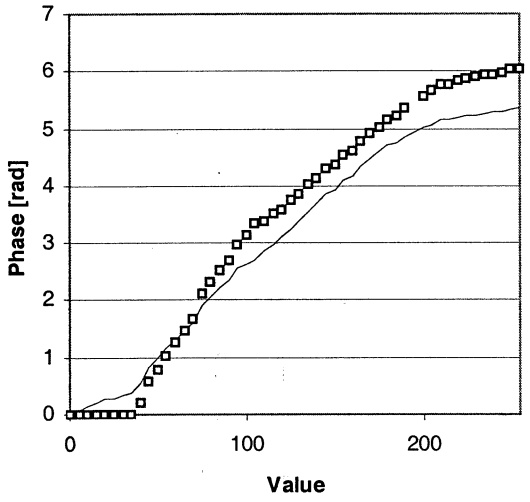

Figure 28 Phase response for the N7 LUT calculated using phase grating method. Squares: only ±1 order included. Solid: ±1 order and zero order included.

5.3 Compensations of the non-linear phase response

A look-up table (LUT) can compensate for a non-linear response observed in a NLC SLM. To construct a new LUT measurements with the rotated polarizers method and the linear LUT was conducted. The phase response was measured for every pixel value between 0 and 127. A polynomial of degree 30 was fitted to the inverse of the measured data (Figure 29).

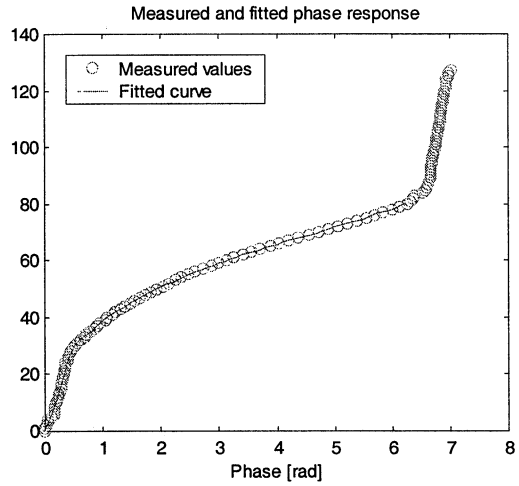

Figure 29 The inverse of the measured phase response and the fitted polynomial.

To check the response of the SLM using this new LUT the rotated polarizer method was utilized. In Figure 30, the resulting phase response is compared with the linear (optimal) and N7 LUT. It can be observed that the new LUT gives a much better phase response compared to N7.

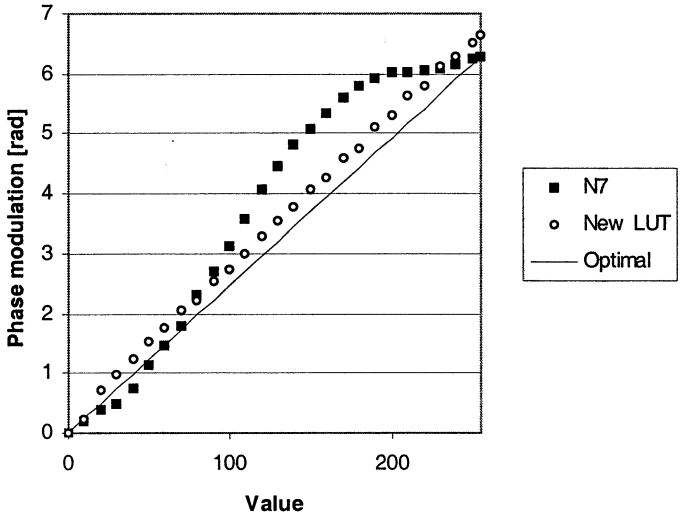

Figure 30 – Phase response for the N7 LUT and the new LUT compared with the optimal linear response.

The phase response with the new LUT was also investigated using the phase grating method. The power observed in the 0:th and 1:st diffraction orders for different values of the phase grating is shown in Figure 31. These results should be compared with the measurements corresponding to the N7 LUT depicted Figure 27.

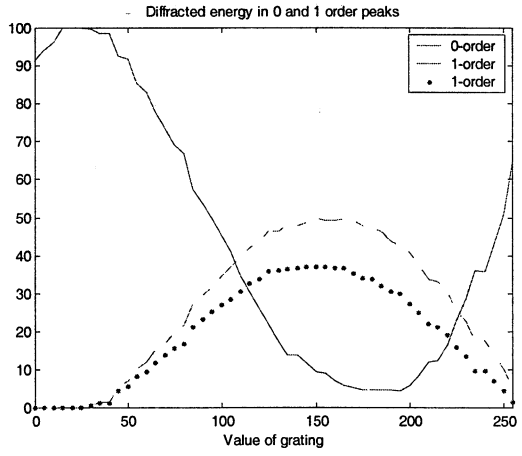

Figure 31 Diffracted energy into the 0:th and 1:st orders when the new LUT was used.

5.4 Measurements of the intensity response

In a pure phase modulation experiment the intensity is not dependent on the applied pixel value. To test if this statement is true image sequences with different pixel values were studied. The average intensity value of each image was calculated. The normalized intensity fluctuation versus the pixel value used to address the SLM for the N7 LUT is shown in Figure 32. As can be seen the reflected intensity seems to vary with the applied voltage.

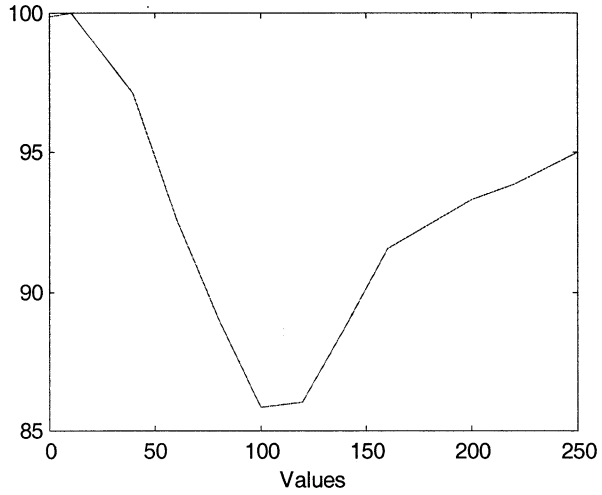

Figure 32 Relative average intensity over the SLM for different values with the N7 LUT.

Hence, a pure phase modulation cannot be observed. Instead the complex modulation of the light is described by the response shown in Figure 33.

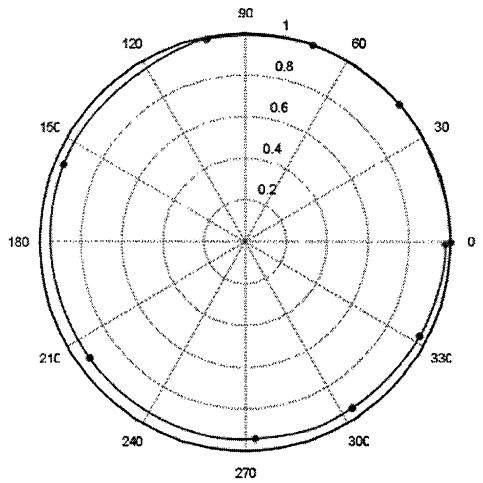

Figure 33 Measured complex response with the new LUT.

6 APPLICATIONS

6.1 Beam steering efficiency

Simple beam steering properties of the SLM have also been studied for the N7 and the optimized LUT. The far field diffraction pattern was measured using binary and blazed gratings (Figure 34). The number of levels in each blazed grating was varied from 2 to 20. The resulting far-field diffraction patterns using the new LUT are shown in Figure 34.

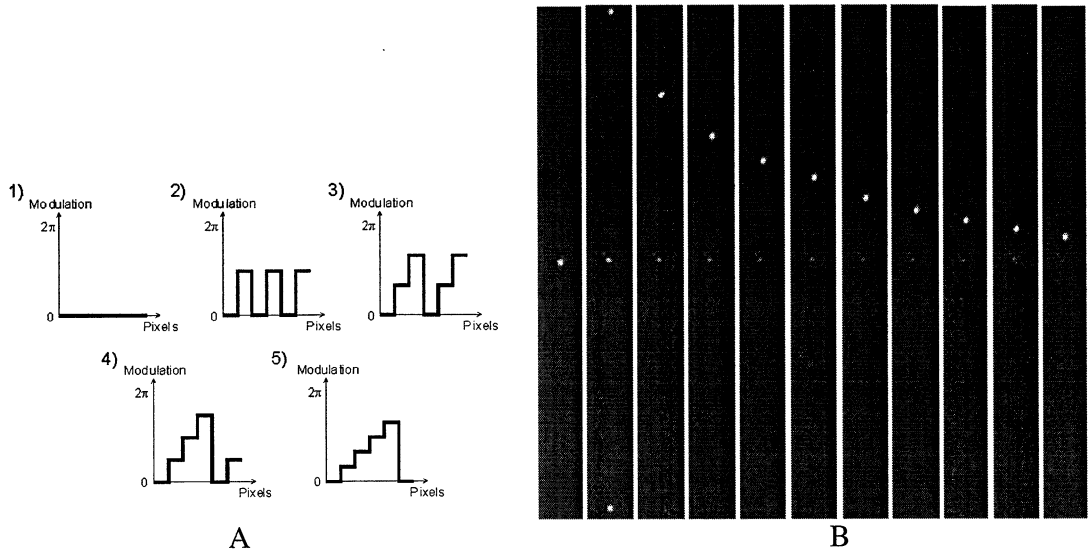

Figure 34 A) The first five blazed gratings used to study the beam steering efficiency for different LUT's. B) Far field diffraction pattern for the blazed gratings in A).

The intensity in the three dominating orders (0, +1 and –1) was summed to give the different diffracted power (Figure 35).

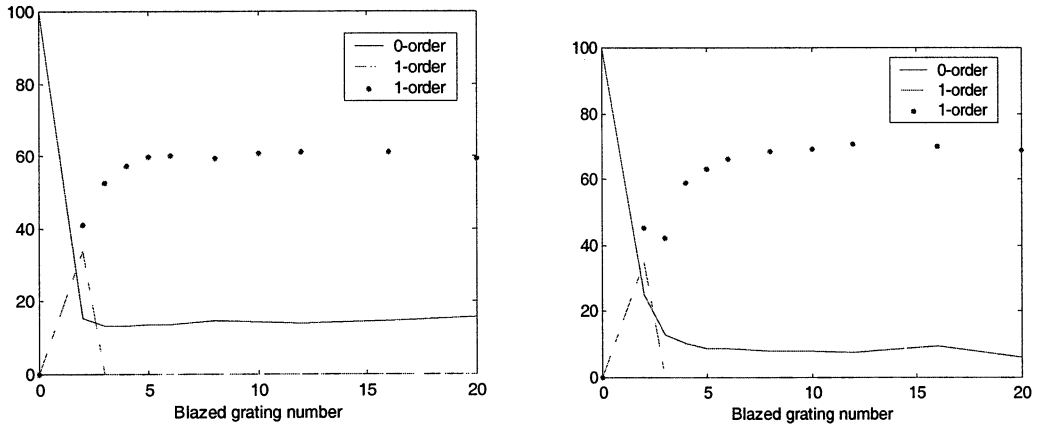

Figure 35 The power diffracted into the 0 and 1 order peaks for the five gratings shown in Figure 34 and the N7 LUT. Sama as (left) but with the optimised LUT (right).

The observed diffraction effect of the blazed grating is higher for the new LUT than for the N7. To further visualize this effect the power in the +1 order has been divided by the power in the 0 order for each grating (Figure 36).

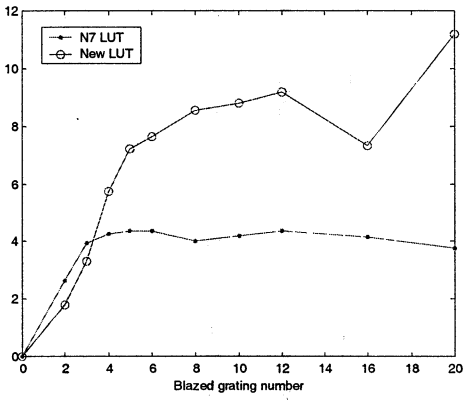

Figure 36 The power diffracted into +1 order divided by the power diffracted into the 0 order.

6.2 Beam shaping

As discussed in chapter 4.5, "Phase retrieval", the phase modulation required on the SLM to give a desired intensity distribution in the far field can be calculated. By using the iterative methods described above the beam can be shaped arbitrary. For example, Gerchberg-Saxton algorithm was used to calculate the phase that produces the letters "FOI" in the far field (Figure 37).

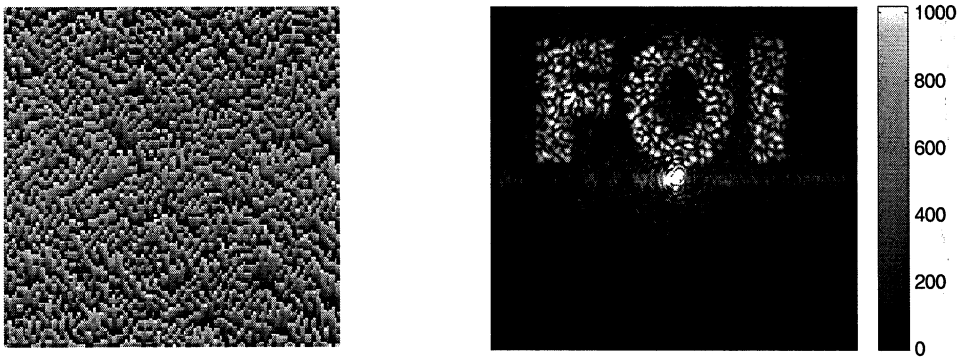

A B

Figure 37 – A) Calculated phase modulation producing the text "FOI" in the far field. B) The intensity pattern registered in the far field using the optimized LUT.

The bright spot in the middle of the image is the zero order peak (or DC component). The speckles are probably due to the fact the plane is sampled into a set of discrete points and between these points destructive interference can occur. By illuminating a larger part of the SLM the point spread function gets narrower and less speckles show up.

In Figure 38 the far field diffraction patterns are shown for the N7 and the new LUT. The scale has been adjusted to make the noise more visible. To get a numerical measurement of the quality of the shaping two areas from each picture were cut out. One part from the background that should be uniformly black indicated by white rectangles in the figures. The second area is indicated by a black rectangle and represents the part of the beam that should be uniformly bright (Figure 38).

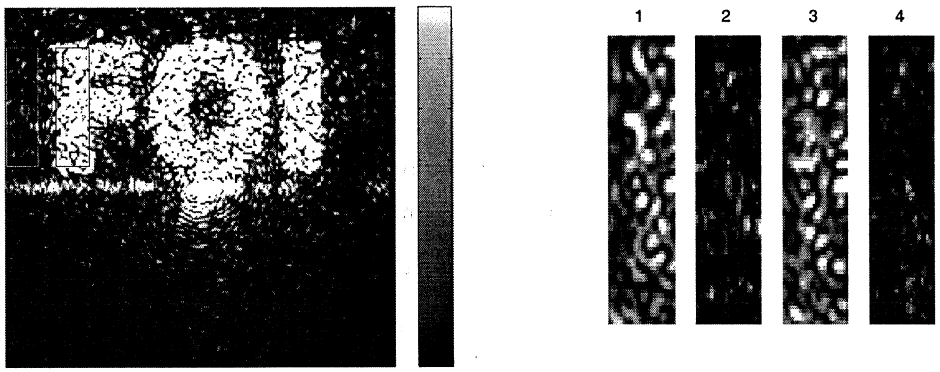

Figure 38 The four images cut out from the rectangles. Images number 1 and 2 are from the N7 image and number 3 and 4 from the new LUT image. Number 1 and 3 are the parts indicated with black boxes and number 2 and 4 with white ones. Observe that the scales are different between the 1-3 pair and the 2-4 pair.

The mean values and standard deviation was calculated for these parts and are presented in Table 1. The optimized LUT results in lower background intensities and higher intensity in the intended region ("F" in this case).

Table 1 Mean value and standard deviations for the images shown in Figure 38.

	Average	Standard deviation
1 -The F – N7 LUT	335	67
3 -The F – new LUT	366	52
2 -Background – N7 LUT	6.6	4.3
4 - Background – new LUT	5.2	2.7

7 DISCUSSION AND CONCLUSION

A method discussed in literature to study the birefringence and the rotation of the extraordinary axis of an SLM was modified to be valid for zero-twist nematic SLM. The experimental parameters were found by fitting theoretical expressions to the measured transmission while rotating polarizers in front and after the SLM. Best fitted values for the rotation of the extraordinary axis in the laboratory frame and the magnitude of the phase delay were presented. These results were obtained with the SLM turned off. Measurements were also performed with the SLM power on and with a uniform voltage applied to all pixels. In this case the same angle of rotation ψ was obtained but the birefringence β varied with the applied voltage as expected. The result of the response measurements with rotated polarizers and the linear LUT showed a non-linear phase response. The N7 look-up table, on the other hand, gives an almost linear phase delay between 0 and 2π. Some non-linearity still remains and a better LUT can be constructed. Measurement of the phase response for the set-up with perpendicular angle of incident was also performed. These experiments showed that the non-linearity for the N7 LUT remained suggesting that the tilt of the SLM and the longer path through the LC is not the origin of the non-linearity. These response results were compared with the phase grating method. It was concluded that the phase grating method is not sufficient to give an accurate phase response. However, the results can be used to get an idea of the phase response or to compare different LUT's. To improve these measurements the CCD camera can be replaced by photodiodes.

A new optimized look-up-table was constructed in this study by taking the inverse of the measured phase response data. From the experimental results with the new LUT a more linear response was observed but with a phase response of less than 2π. It can also be noted that the $0/\pi$ binary grating resulted in a diffraction efficiency of about 40% into +1 and –1 diffraction orders, respectively. This agrees with the theoretical predicted efficiency of 40.5 %. To study the amplitude response the result form the interferometer analyze was used. The average values of these images while the value on the SLM was changed are shown in Figure 32. The amplitude response measurements indicate that a pure phase modulation not is obtained. Instead a coupled phase-amplitude response is presence.

To study the effect of a non-linear phase response in beam steering and beam shaping measurements were performed with different LUT's. The intensity steered to the first order is divided by the intensity in the zero order for different blazed gratings. These results showed that the blazed grating with 20 levels gives approximately 4 times more power in the first than in the zero diffraction order using the N7 LUT. If the optimized LUT was utilized 11 times more power was observed in the first order. Comparing the results for the $0/\pi$ phase grating indicates that the efficiency can be further increased. From these results the maximum efficiency for the $0/\pi$ phase grating was 7 for the N7 and 9 for the optimized LUT. Finally, it was shown that the new LUT give improved beam shaping properties.

8 REFERENCES

1. U Efron, "Spatial light modulator technology", Marcel Dekker Inc., US 1995
2. C Soutar, K Lu, "Determination of the physical properties of an arbitrary twisted-nematic liquid crystal cell", Opt. Eng. Vol. 33(8), p2704-2712 (1994)
3. E Collett, "Polarized light", Marcel Dekker Inc., US 1993
4. J.W. Goodman, "Introduction to Fourier optics", McGraw-Hill, Singapore 1996
5. J A Davis, D B. Allison, K G D'Nelly, M L Wilson, I Moreno, "Ambiguities in measuring the physical parameters for twisted-nematic liquid crystal spatial light modulators", Opt. Eng. Vol 38(4), p705-709 (1999)
6. J A Davis, P Tsai, K G D'Nelly, I Moreno, "Simple technique for determining the extraordinary axis direction for twisted-nematic liquid crystal spatial light modulators", Opt.Eng. 38(5), p929-932 (1999)
7. M.O. Freeman, T.O. Brown, D,M, Walba, "Quantized complex ferroelectric liquid crystal spatial light modulators", Appl. Opt. Vol 31(20), p3917-3929 (1992)
8. N Mukohzaka, N Yoshida, H Toyoda, Y Kobayashi, T Hara, "Diffraction efficiency analysis of a parallel-aligned nematic-liquid-crystal spatial light modulator", Appl. Opt. Vol. 33(14), p2804-2811 (1994)
9. A Bergeron, J Gauvin, F Gagnon, D Gingras, H Arsenault, M Doucet, "Phase calibration and applications of a liquid crystal spatila light modulator", Appl. Opt. Vol 34(23), p5133-5139 (1995)
10. P Grother, D. Casasent, "Optical path difference measurement techniques for SLMs", Opt. Comm. 189, p31-38 (2001)
11. J Davis, P Tsai, D Cottrell, T Sonehara, J Amako, "Transmission variations in liquid crystal spatial light modulators caused by interference and diffraction effects", Opt. Eng. 38(6), p1051-1057 (1999)
12. H. Dammann, "Spectral characteristics of stepped-phase gratings", Optik 53, p409-417 (1979)
13. B Löfving, "Measurement of the spatial phase modulation of a ferroelectric liquid-crystal modulator", Appl. Opt. Vol 35 (17), p3097-3103 (1996)
14. R W Gerchberg, W O Saxton, "A practical algorithm for the determination of phase from image and diffraction plane pictures", Optik 35, p237-246 (1972)
15. J R Fienup, "Phase retrieval algorithms: a comparison", Appl. Opt. Vol 21 (15), p2758-2769 (1982)